Eur. Phys. J. Special Topics **213**, 213–224 (2012)

DOI: 10.1140/epjst/e2012-01672-5

THE EUROPEAN PHYSICAL JOURNAL SPECIAL TOPICS

Review

Synchrotron X-rays and neutrons as essential tools in Li battery research: Examples of oxide, phosphate and silicate-based positive electrodes

C. Masquelier

LRCS, Université Picardie Jules Verne, 33 rue Saint-Leu, 80039 Amiens, France

Received 22 September 2012 / Received in final form 27 September 2012
Published online 3 December 2012

Abstract. The precise characterization and structural analysis of positive electrodes for Li-ion batteries is essential for the development of long-life, safe and high-energy electrochemical systems. For this purpose X-Ray and neutron diffraction have proved to be essential tools in evaluating pristine powder materials (purity, cation ordering and distribution, defects) as well as the mechanisms (single-phase vs. two-phase reactions) of Li^+ insertion/extraction in and out of these electrodes. This contribution focuses on the illustration of case-studies of structural considerations in oxides, phosphates and silicates of transition metal elements and lithium recently developed, in particular $LiMn_2O_4$, $LiMPO_4$ and Li_2MSiO_4 (M = Fe, Mn).

1 Introduction

Besides the fast-growing development of portable electronic devices (mobile telephones, microcomputers, video cameras, electronic plays...) during the twenty last years, important environmental issues and the pressure of the automobile industry to commercialize hybrid or full electric vehicles have made the development of rechargeable batteries with high energy density and low mass, a worldwide imperative [1]. Lithium batteries are at the centre of an intense fundamental and industrial research since the commercialization of the first ion-lithium rechargeable battery by Sony-Energy in 1991 [2]. The fundamental physics and chemistry of these batteries is based on the electrochemical change of the Li-content in the electrode materials, i.e. the reversible insertion or 'intercalation' of Li ions in compositions such as the intensively studied $LiCoO_2$ [3] which has been developed as a standard positive electrode for more than 20 years. Li^+ insertion/extraction has to proceed reversibly in/out of the electrode materials, associated with the reduction/oxidation of the transition metal element to yield/accept electrons. In this regard, the choice of the material (oxides, poly-anions ...) and its structural properties (distortions, layered or 3-D framework, structural rigidity, behavior under Li^+ (des)insertion ...) during the electrochemical process is one key-factor.

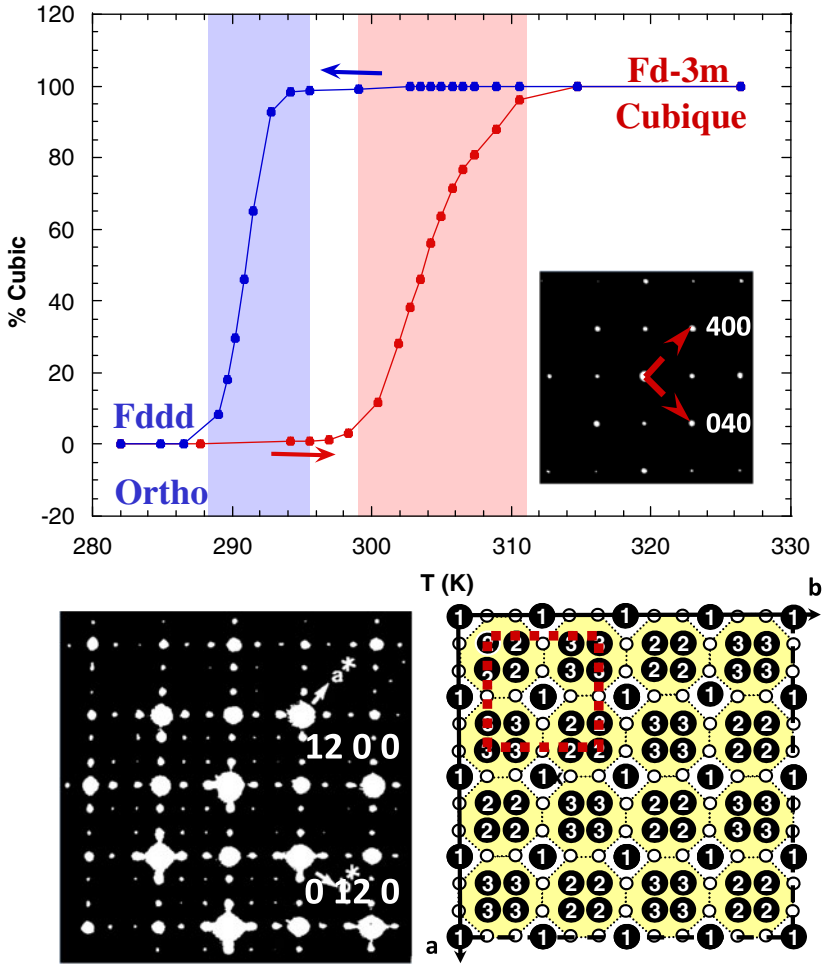

Fig. 1. Illustration of the charge-ordering transition in stoichiometric $LiMn_2O_4$. Top: evolution of the cubic vs. orthorhombic ratio as a function of temperature on heating and on cooling, as deduced from refinements of temperature-dependant X-Ray Synchrotron data. Lower part, left: electron diffraction photograph of superstructure reflections spotted for the charge-ordered form. Lower Part, right: distribution of Mn crystallographic sites in the orthorhombic superstructure of $LiMn_2O_4$. Numbers 1, 2 & 3 figure refer to Mn^{3+} sites, Mn1, Mn2 and Mn3.

2 Charge ordering in $LiMn_2O_4$

Oxides of transition metal elements, such as Li_xMO_2 (M = Co, Ni, Mn), $Li_xMn_2O_4$, $Li_xV_2O_5$ or $Li_xV_3O_8$ have been the most widely studied positive electrode materials as they operate on the M^{5+}/M^{4+} or M^{4+}/M^{3+} redox couples, in between 3V and 5V vs. Li^+/Li thus providing high energy density to the associated Li-ion electrochemical cell. Recently developed "layered" materials for applications include $LiNi_{0.80}Co_{0.15}Al_{0.05}O_2$ [4], $LiCo_{1/3}Ni_{1/3}Mn_{1/3}O_2$ [5], $LiMn_{0.5}Ni_{0.5}O_2$ and $xLi_2MnO_3.(1\text{-}x)LiMO_2$ [6,7]. Their 2-D structure, although being favourable for Li^+ diffusion, may lead to structural instabilities when the number x of extracted lithium is high (end of charge). The 3-D spinel compound $LiMn_2O_4$, early proposed by

Thackeray and Goodenough [8] and M.M. Thackeray [9–11] remains a very interesting electrode material and initiated immense research activity, with the recent development, for instance, of $Li[Ni_{0.5}Mn_{1.5}]O_4$ that operates at about 4.7 V vs. Li [12]. MnO_6 octahedra are connected to each other through edge-sharing and delimitate a three-dimensional network of conduction paths for lithium motion.

Despite its apparent simplicity, the crystal structure of the spinel $LiMn_2O_4$ was widely investigated by many groups. We illustrate here the work performed by Rousse et al. on the finding of a new superstructure due to partial charge ordering in stoichiometric $LiMn_2O_4$ [13–15]. Depending on the chemistry used (stoichiometry of precursors, temperature, O_2 partial pressure) $LiMn_2O_4$, can undergo significant departure from its ideal stoichiometry for which the average oxidation state of Mn is 3.5+ [16]. Thackeray et al. have extensively reviewed [17–19] the formations of $Li_{1+x}Mn_{2-x}O_4$ ($0 \leq x \leq 0.33$, i.e. solid solution between $LiMn_2O_4$ and $Li_4Mn_5O_{12}$) and $Li_{1-y}Mn_{2-2y}O_4$ ($0 \leq y \leq 0.11$, i.e. solid solution between $LiMn_2O_4$ and $Li_2Mn_4O_9$)). Under precise conditions, it is possible to prepare rigorously stoichiometric powders of $LiMn_2O_4$ which were subsequently found to undergo a structural phase transition close to room temperature from cubic to orthorhombic symmetry [15] (Fig. 1). Electron diffraction at 230 K revealed a $\sim 3a \times 3a \times a$ superstructure of the cubic spinel structure (space group *Fddd,* a=24.743(1), b=24.840(1), c=8.199(1) Å)) that was later on found, through temperature-controlled neutron diffraction, due to charge ordering on the manganese sites [13]. Additionnally, temperature-controlled Synchrotron X-Ray diffraction allowed to prove unequivocally that the charge ordering-disordering transition was of first-order with the coexistence of two phases in a small range of temperatures and a significant hysteresis on cooling [14]. The orthorhombic phase isolated at 230K progressively shifts to a symmetry close to tetragonal when cooled down to lower temperatures.

3 Crystal structure and magnetic ordering in $LiFePO_4$ and its delithiated form $FePO_4$

Besides transition metal layered or spinel oxides, three-dimensional frameworks built on transition metals and polyanions $(XO_4)^{n-}$ have become in the last fifteen years the subject of very intensive research worldwide since the discovery of the electrochemical activity of olivine-type $LiFePO_4$ [20,21]. These materials provide very stable frameworks that allow long term structural stability, essential for extensive cycling and safety issues and, depending on the chemical nature of the polyanion, may operate at a relatively high voltage vs. Li for a given $M^{n+}/M^{(n-1)+}$ redox couple, when compared with oxides. Lithium can be extracted reversibly from the triphylite $LiFePO_4$ at ~3.5 V vs. Li^+/Li and it quickly became the material of choice for Li insertion/extraction among the so-called polyanionic structures [22].

Triphylite $LiFePO_4$ adopts the olivine structure-type, described using an orthorhombic unit-cell in either the Pmnb or Pnma (equivalent) space groups (a =10.338(1) Å, b =6.011(1) Å, c =4.695(1) Å in Pnma description). The framework is built on distorted oxygen hexagonal packing into which Li^+ and Fe^{2+} occupy half of the octahedral sites and P occupies $1/8^{th}$ of the tetrahedral sites [23,24]. The peculiar distribution of Li^+ and Fe^{2+} within the octahedral sites has a special impact on both electronic and ionic conductivities. FeO_6 octahedra share corners between each other, not edges, and electronic delocalization is hence difficult. The average Fe^{II}-O distance is much higher than what is expected for Fe^{2+} in octahedral coordination, probably due to the fact that the FeO_6 octahedra share edges with PO_4 tetrahedra [25]. As a consequence, electrostatic repulsions between Fe and P ions weaken the Fe-O bond strength, which is at the origin of the unusually high operating voltage of

this electrode material when lithium ions are extracted from the framework (3.45 V *vs* Li+/Li). Lithium is located in a second set of octahedral sites but distributed differently: LiO_6 octahedra share edges in order to form LiO_6 chains running parallel to $[100]_{Pmnb}$ which generates, according to Morgan and Ceder [26], preferential rapid one-dimensional Li^+ ion conductivity along that direction.

Through electrochemical or chemical oxidative reactions, the delithiated form, $FePO_4$, of triphylite $LiFePO_4$ can be easily prepared, where the respective positions of Fe and P atoms are essentially unchanged. The structure of $FePO_4$ is basically the same as that of $LiFePO_4$, but with anisotropic lattice parameters variations: contraction along [100] and [010] and, more intriguing, slight elongation along [001] [25]. As for $LiFePO_4$, the unique Fe atom is located at the middle of an FeO_6 octahedron, which is more distorted than in $LiFePO_4$. The Fe-O distances range from 1.89(1) to 2.13(1) Å, with an average distance of 2.015(1) Å, in good agreement with the expected value for iron in the oxidation state +3.

Noticeably, this structural type had been first investigated for its magnetic properties [23,24,27,28] and temperature-controlled neutron diffraction on polycrystalline samples was subsequently used by Rousse et al. to draw for the first time a close comparison between the magnetic structures of $LiFe^{II}PO4$ and $Fe^{III}PO_4$ [25]. Both compounds show antiferromagnetic behavior below 52 K for $LiFePO_4$ (Fe^{2+}) and below 125 K for $FePO_4$ (Fe^{3+}), characterized by the appearance of extra peaks in the neutron diffraction patterns below the Néel temperature (Fig. 2). Interestingly, the orientation of the magnetic moments are rotated by $\partial/2$ when lithium is extracted, from a collinear solution along the *b*-axis in $LiFePO_4$ to a non-collinear solution mainly along the *a*-axis (plus a minor component along the *b*-axis) in $FePO_4$: the magnetic moments of the four iron atoms present in the unit cell are oriented along [010] for $LiFePO_4$ and mostly along [100] (with a small component along [010]) for $FePO_4$. The magnetic structures and the differences in the Néel temperatures were discussed in terms of super and super-super exchange interactions and of anisotropy of Fe^{2+} [25].

4 Formation of a complete Li_xFePO_4 solid solution

The electrochemical extraction of Li^+ from stoichiometric, micro-sized crystalline powders of $LiFePO_4$ was initially thought to proceed through a straightforward two-phase reaction between $LiFePO_4$ and $FePO_4$ end members. Early careful Rietveld refinement of X-ray powder diffraction investigations performed by Yamada [29] revealed that the reaction indeed proceeds with slight deviation of the orthorhombic lattice constants from those of the stoichiometric end members. Yamada et al. hence proposed the existence of spinodal-type system where the intermediate Li_xFePO_4 $\alpha < x < 1–\beta$ region consists actually in $Li_\alpha FePO_4$ and $Li_{1-\beta}FePO_4$ mixtures where $\alpha = 0.032$ and $\beta = 0.038$ at room temperature. Later on Kobayashi proposed that the values of α and β could vary significantly as a function of $LiFePO_4$ particles size: the smaller the particle size, the bigger α and β [30].

Delacourt et al. investigated the thermal behavior of x $LiFePO_4 + (1 - x)$ $FePO_4$ mixtures ($0 \leq x \leq 1$) through temperature-controlled X-Ray diffraction under N_2 and revealed the existence of complete Li_xFePO_4 solid solutions over the entire composition $0 \leq x \leq 1$ range for $\sim 350 < T <\sim 500\,^\circ C$, the olivine-type framework of the triphylite being maintained [31]. Remarkably, as soon as the temperature is raised from 25 °C to about 200 °C, Li^+ ions diffusion from $LiFePO_4$ to $FePO_4$ is possible, leading to the transformation of the two-phase mixtures of x $LiFePO_4$ and (1-x) $FePO_4$ into a new equilibrium state for which phase of intermediate composition, Li_xFePO_4, is stable ($0 \leq x \leq 1$) [31,32]. Subsequently, Delacourt et al. investigated the crystal

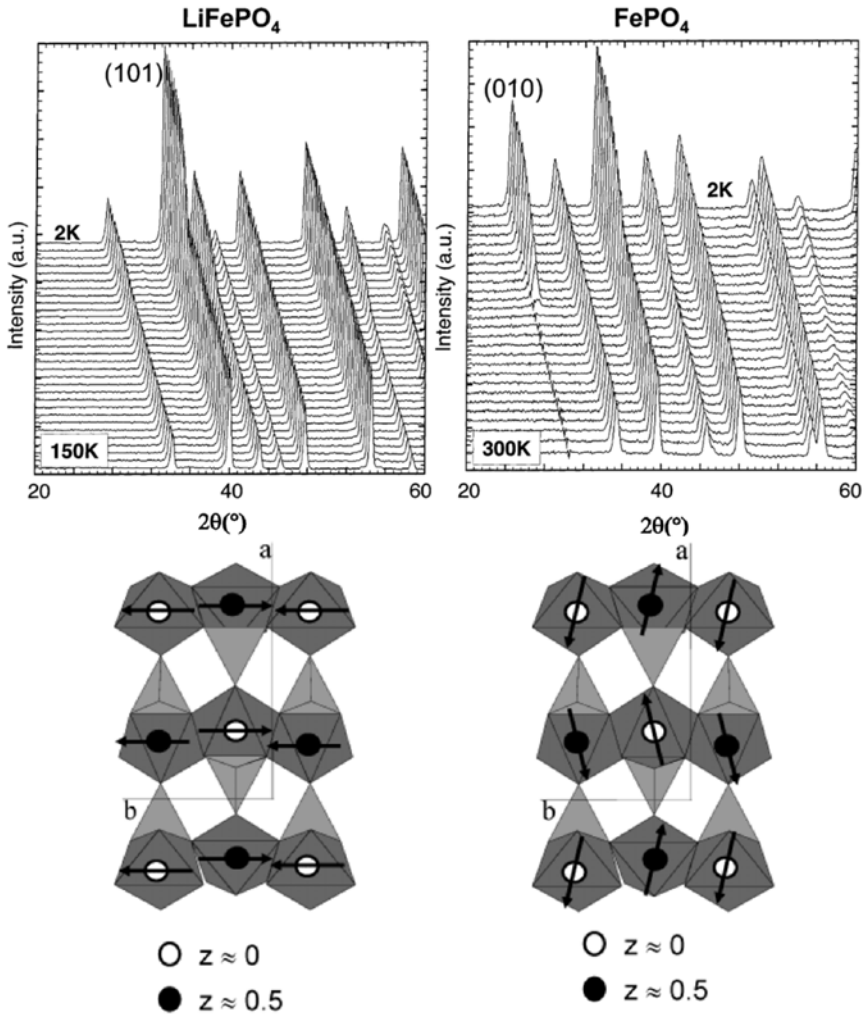

Fig. 2. Top: temperature-controlled neutron diffraction experiments on $LiFePO_4$ and on its delithiated form $FePO_4$. Bottom: representations of the antiferromagnetic structures.

chemistry of a 0.5 $LiFePO_4$ + 0.5 $FePO_4$ mixture upon heating at 350 °C and then upon cooling at room temperature, through neutron and synchrotron X-ray diffraction [33]. The Rietveld refinement of the neutron diffraction data of the single phase $Li_{0.5}FePO_4$ obtained at 350 °C (Fig. 3) converges towards unit-cell parameters intermediate between those of the two isostructural end-members, $LiFePO_4$ and $FePO_4$ and to a global occupancy of the Lithium site of 0.45(4). The average Fe-O distance was found, moreover, consistent with the existence of a mixed-valence Fe(II)-Fe(III) solid solutions, as confirmed by a bond valence sum of 2.40(1). Significant anisotropic micro-strains, within the $(001)_{Pmnb}$ planes, were found, likely as the result of heterogeneous distance distributions within the 1-D $[100]_{Pmnb}$ Li^+ conduction channels and between these channels along $[010]_{Pmnb}$. Later on, Yamada confirmed the existence of this solid solution and provided, through careful refinement of anisotropic displacement parameters, a nice visualization of the 1-D Lithium diffusion channels in the triphylite framework [34].

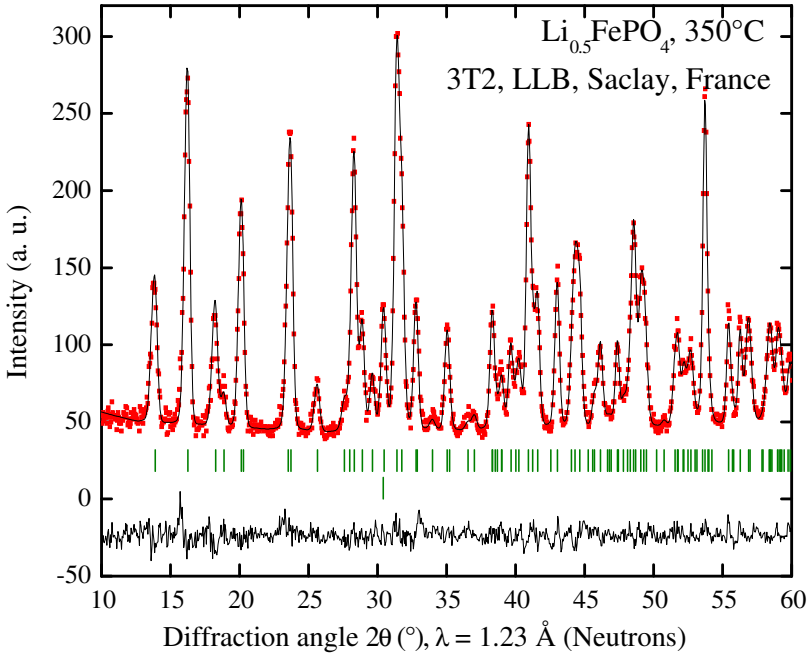

Fig. 3. Rietveld refinement of neutron diffraction data for single-phase $Li_{0.5}FePO_4$ at 350 °C.

On cooling, the behavior of the Li_xFePO_4 solid solution was found to be more complicated than on heating, resulting in mixtures of phases depending on x, as well as on the thermal history of the samples [33]. On the contrary with what happens during the heating sequence the de-mixing of Li_xFePO_4 single phases upon cooling was shown to be much composition sensitive and at room temperature, mixtures of olivine-type phases were constantly obtained: the two end-members $LiFePO_4$ and $FePO_4$ as well as metastable phases may kinetically coexist with compositions close to $Li_{0.5}FePO_4$ and $Li_{0.75}FePO_4$.

5 Structural defects in $Li_xFe_yPO_4$

In order to compensate the low intrinsic transport properties of $LiFePO_4$, many groups worldwide developed a myriad of synthesis techniques aimed at producing nano-sized powders with superior rate performances [35–44]. Among these, Delacourt developed solution based procedures that allowed the direct precipitation, into DMSO–H_2O mixtures at ∼100 °C under ambient pressure, of "$LiFePO_4$" particles with various morphologies and sizes, depending on the time of precipitation and concentration of precursors [45]. A systematic crystallographic study of various "generations" of powders was undertaken leading to the important observation, first, of significant lattice parameter variations (contractions) in 40 nm-size particles [46]. Consistently, powders prepared by low temperature technique, were found to possess a unit-cell volume close to 289 $Å^3$ that would, through a linear extrapolation between the referenced unit-cell volumes of $LiFePO_4$ and $FePO_4$, correspond to an x value of ∼0.85 in Li_xFePO_4. Careful Rietveld analyses of both X-ray and neutron diffraction data revealed for the first time important departures from the ideal $Li_{1.00}Fe_{1.00}PO_4$ stoichiometry and converged, in full coherence with atomic absorption chemical analysis and Mossbauer spectroscopy towards

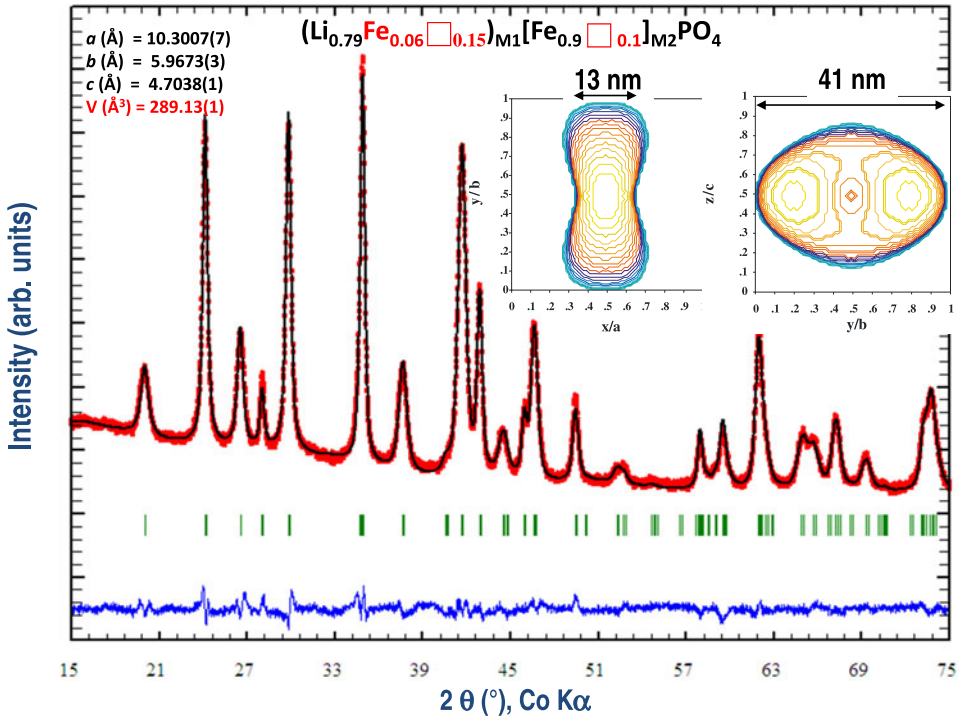

Fig. 4. Rietveld refinement of X-Ray diffraction data for defective $LixFeyPO_4$. The insert refers to anisotropic diffraction peak broadening refinement leading to the crystallite coherence lengths given.

the chemical formula $(\square_{0.15}Li_{0.79}Fe_{0.06})_{M1}(\square_{0.10}Fe_{0.90})_{M2}PO_4$ (Fig. 4): this highlighted the existence of both cation vacancies and inter-sites mixing within the structure "LiFePO4" nano-powders, in agreement with atomistic calculations of Islam et al. [47–49] who predicted that such defects might indeed be intrinsic to $LiFePO_4$. Later on, experimental visualization of Fe atoms sitting onto Li sites was reported by Chung et al through neutron diffraction and aberration corrected STEM [50].

The most striking feature of the electrochemical data obtained upon extraction of Li^+ from this highly-defective $Li_xFe_yPO_4$ composition is the observation of a sloping voltage curve as a function of remaining Li^+ content which contrasted with all previous data reported for "$LiFePO_4$". Sloping voltage composition curves are usually characteristic of single phase Li de-intercalation / intercalation mechanisms. *In situ* X-ray diffraction measurements were hence performed and demonstrated a reversible slight and continuous shift in the Bragg peaks, signature of a full solid solution with lattice parameters variations that follow nicely the Vegard's law [46].

These findings have pointed out that the electrochemical properties of $LiFePO_4$ electrodes could be, besides straightforward size effects, strongly influenced by the presence of chemical/structural defects generated by low temperature synthesis techniques aimed at producing small particles. A rich illustration was provided by the recent work of Hamelet [51,52] who found that gentle annealing of $LiFePO_4$ in air (100 °C to 400 °C) would generate major cations distribution rearrangements within the $LiFePO_4$ structure and completely new mechanisms of Li^+ insertion/extraction. Combined investigations using Mossbauer and NMR spectroscopies

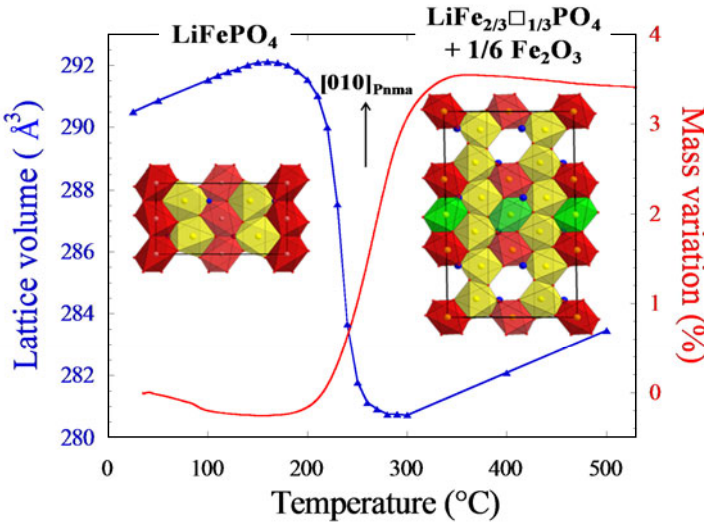

Fig. 5. Mass variation and unit-cell volume variation as a function of temperature during annealing of $LiFePO_4$ in air.

besides T-controlled X-Ray and Neutron diffraction, demonstrated that the oxidation of $LiFePO_4$ in air at 180–400 °C (accompanied by significant mass gain, see Fig. 5) leads to the extrusion of Fe towards the particle surface and hence to Fe vacancies. It was then possible to obtain a pure Fe^{III} olivine, where 1/3 of the iron initially contained in the $LiFePO_4$ pristine particles had been extruded to form nano-clusters of Fe_2O_3. Complex and new redox phenomena are then associated with the Li^+ insertion/extraction into/from these new highly defective "$LiFe_yPO_4$" compositions.

Recently [52], Hamelet et al. further demonstrated that Fe atoms are redistributed onto the M(1) and M(2) crystallographic sites of the triphylite framework and lead, when significant amounts of Fe vacancies have been created, to complex superstructures similar to what had been previously described for the transformation of fayalite to laihunite [53,54].

6 Polymorphism of Li_2FeSiO_4

Lithium transition metal silicates, with a general formula Li_2MSiO_4 (M = Fe, Mn, Co), are considered as attractive positive electrode material due to the theoretical possibility to exchange two mol of lithium per formula unit [55–57]. The abundance of raw materials (particularly true for Fe and Si) and the reversibility of the Fe^{II}/Fe^{III} redox couple are attractive attributes for Li_2FeSiO_4 to be chosen as a cathode material for large scale battery applications.

Their crystal structure consists of slightly distorted close packed oxygen slabs between which cations occupy only tetrahedral sites [58]. As reviewed recently by Sirisopananporn et al. [59–61] and Nishimura [62], Li_2MSiO_4 compositions may crystallize within different crystallographic polymorphs, depending on the synthesis parameters [63]. Their crystal structures are derived from the low and high temperature forms of Li_3PO_4 [64–66]. Polymorphs of Li_2FeSiO_4 crystallizing in $Pmn2_1$ (LFS@400, i.e. prepared at 400 °C), in $P2_1/n$ (LFS@700) and Pmnb (LFS@900) space groups were successfully isolated (Fig. 6).

The difference in their structure is based on the orientation/distribution of cations over half of the available tetrahedral interstices, generated by distorted hexagonal

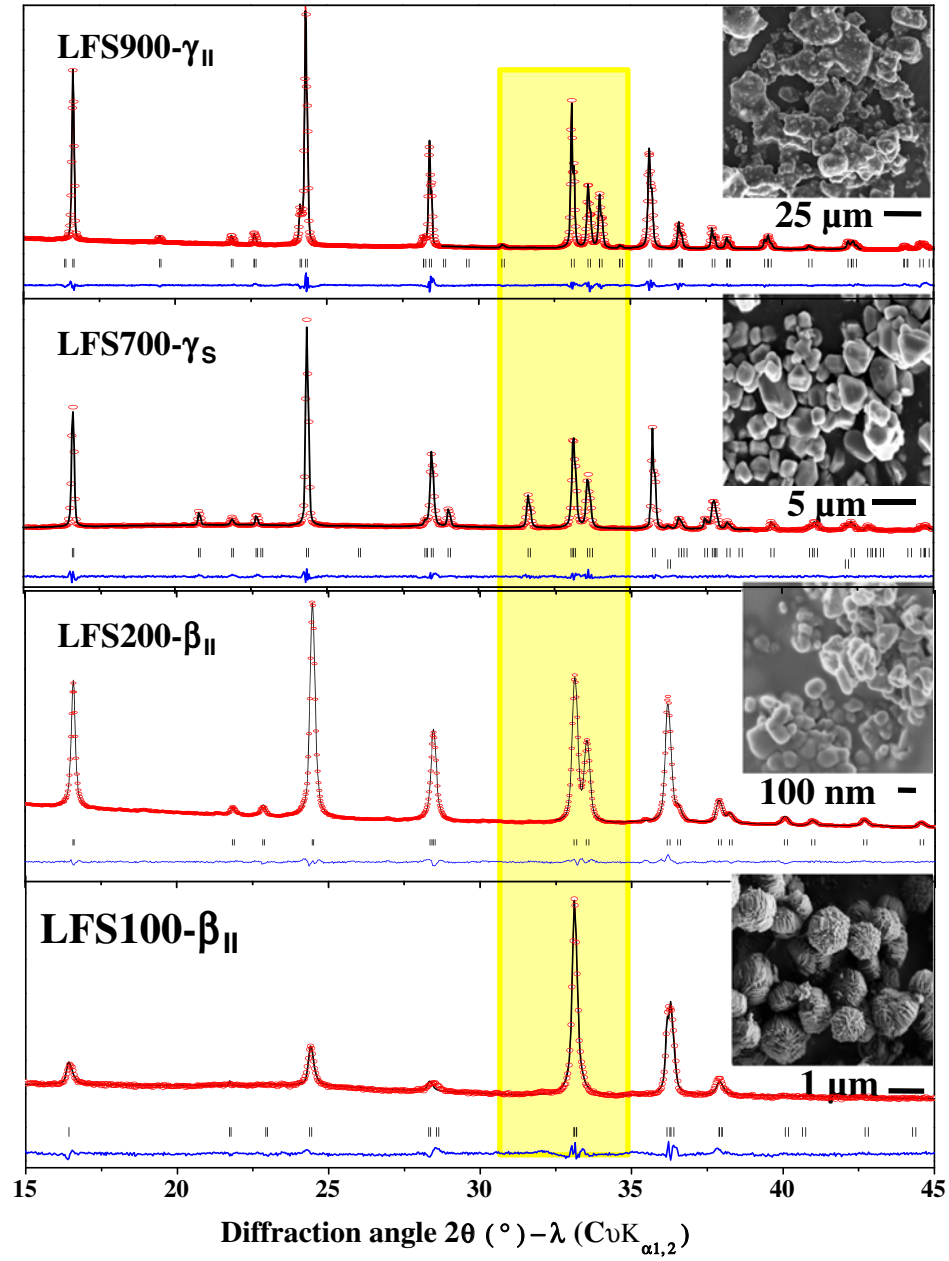

Fig. 6. Full pattern matching refinement of X-Ray diffraction data for the different polymorphs of Li_2FeSiO_4 isolated.

close-packed arrays of oxygen layers. Local structures of FeO_4 and LiO_4 tetrahedra differ from one polymorph to another as well as their interconnectivity with adjacent MO_4 tetrahedra and in their respective orientations along a given crystallographic direction. The structural variations affect the average Fe-O bond lengths, the distortion of the FeO4 tetrahedra, and the connectivity-scheme between LiO_4 and FeO_4 tetrahedra among the three structures. The increase in Fe-O bonds and the decrease in FeO_4 distortion from the γII to βII consequently gives rise to the increase in the isomer

shifts and quadrupole splitting values deducted from their corresponding Mössbauer spectra [60].

Importantly, variations around the FeO_4 arrangements (orientation, size, and distortion) do influence the equilibrium potentials during the first oxidation in all polymorphs. The shorter (stronger) Fe-O bonds result in higher splitting energy between bonding and antibonding states, and thus diminishing the difference between Fe^{2+}/Fe^{3+} and Li+/Li° redox values [61]. In addition the phase transformation kinetics of Li_2FeSiO_4 upon lithium extraction/ insertion are structural, cycling-rate and temperature dependent.

7 Conclusion

The above-mentioned examples were selected as interesting illustrations, among many others, of the richness of the crystal chemistry of materials used as positive electrodes for Li-ion batteries. X-ray and neutron diffraction have proven to be essential techniques in the design and characterization of such materials as well as in the study of Li+ insertion/extraction mechanisms through post-mortem analysis or in situ measurements during electrochemical operation. Large-scale synchrotron facilities in Japan, USA, Australia and Europe are welcoming many scientists for fast and very high resolution diffraction measurements on battery materials. In operando investigations (at and out of equilibrium) are becoming more and more popular as well and generate (besides enormous amounts of data that need to be carefully analyzed....) very useful insights into how battery materials do operate, once reliable electrochemical cells can be implemented for such kind of measurements [67]. Related to neutron scattering issues, more limited work has been published due to the inherent difficulties associated with the need of larger amounts of powder samples and with the presence of hydrogen-containing liquid electrolytes. However, very recent successful demonstration of full-cell operando measurements of commercial batteries within a neutron beam [68] opens the door for exciting developments in battery "autopsy" to researchers from both the academic and industry worlds.

The author wishes to acknowledge, for the studies presented above, the essential contributions of G. Rousse, C. Wurm, S. Patoux, C. Delacourt, G. Quoirin, S. Hamelet and C. Sirisopanaporn as well as fruitful collaborations with J. Rodriguez-Carvajal, E. Elkaïm, S. Levasseur, M. Casas-Cabanas, R. Dominko, D. Bonnin, L. Croguennec, A. Boulineau, M. Morcrette P. Poizot and J.M. Tarascon. The Laboratoire Léon Brillouin (LLB, Saclay, France), the Institut Laüe Langevin (ILL, Grenoble, France), the synchrotron SOLEIL (Gif-sur-Yvette, France) and the Paul Scherrer Institut (PSI, Switzerland) are gratefully acknowledged for allocated beam time and their technical support.

References

1. J.M. Tarascon, M. Armand, Nature **414**, 359 (2001)
2. M.S. Whittingham, Chem. Rev. **104**, 4271 (2004)
3. K. Mizushima, P.C. Jones, P.J. Wiseman, J.B. Goodenough, Mater. Res. Bull. **15**, 783 (1980)
4. M. Guilmard, C. Pouillerie, L. Croguennec, C. Delmas, Solid State Ionics **160**, 39 (2003)
5. T. Ohzuku, Y. Makimura, Chem. Lett. **30**, 642 (2001)
6. Z.H. Lu, D.D. MacNeil, J.R. Dahn, Electrochem. Solid-State Lett. **4**, A191 (2001)
7. M.M. Thackeray, C.S. Johnson, J.T. Vaughey, N. Li, S.A. Hackney, J. Mater. Chem. **5**, 2257 (2005)

8. J.B. Goodenough, M.M. Thackeray, W.I.F. David, P.G. Bruce, Rev. Chim. Minér. **21**, 435 (1984).
9. M.M. Thackeray, W.I.F. David, J.B. Goodenough, Mater. Res. Bull **17**, 785 (1983)
10. M.M. Thackeray, W.I.F. David, P.G. Bruce, J. B. Goodenough, Mater. Res. Bull **18**, 461 (1983)
11. M.M. Thackeray, P.J. Johnson, L.A. de Picciotto, P.G. Bruce, J.B. Goodenough, Mater. Res. Bull **19**, 179 (1984)
12. M. Imazaki, K. Ariyoshi, T. Ohzuku, J. Electrochem. Soc. **156**, A780 (2009)
13. J. Rodriguez-Carvajal, G. Rousse, C. Masquelier, M. Hervieu, Phys. Rev. Letters **81**, 1460 (1998)
14. G. Rousse, C. Masquelier, J. Rodriguez-Carvajal, E. Elkaim, J.P. Lauriat, J.L. Martinez, Chem. Mater. **11** 3629 (1999)
15. G. Rousse, C. Masquelier, J. Rodriguez-Carvajal, M. Hervieu, Elec. Solid State Lett. **2**, 6 (1999)
16. C. Masquelier, M. Tabuchi, K. Ado, R. Kanno, Y. Kobayashi, Y. Maki, O. Nakamura, J.B. Goodenough, J. Solid State Chem. **123**, 255 (1996)
17. M.M. Thackeray, M.H. Rossouw, A. de Kock, A.P. de la Harpe, R.J. Gummow, K. Pearce, D.C. Liles, J. Power Sources **43–44**, 289 (1993)
18. R.J. Gummow, M.M. Thackeray, J. Electrochem. Soc. **141**, 1178 (1992)
19. R.J. Gummow, D.C. Liles, M.M. Thackeray, Mater. Res. Bull. **28**, 1249 (1993)
20. A.K. Padhi, K.S. Nanjundaswamy, J.B. Goodenough, J. Electrochem. Soc. **144**, 1188 (1997)
21. A.K. Padhi, K.S. Nanjundaswamy, C. Masquelier, S. Okada, J.B. Goodenough, J. Electrochem. Soc. **144**, 1609 (1997)
22. J.B. Goodenough, Y.J. Kim, Power Sources **196**, 6688 (2011)
23. P.R. Santoro, R.E. Newnham, Acta Cryst. **22**, 344 (1967)
24. M. Mercier, P. Bauer, B. Fouilleux, C.R. Acad. Sci. **267**, 1345 (1968)
25. G. Rousse, J. Rodriguez-Carvajal, S. Patoux, C. Masquelier, Chem. Mater. **15**, 4082 (2003)
26. D. Morgan, A. Van der Ven, G. Ceder, Electrochem. Solid State Lett. **7**, A30 (2004)
27. S. Geller, J.L. Durand, Acta Cryst. **13**, 325 (1960)
28. A. Goni, L. Lezama, G.E. Barberis, J.L. Pizarro, M.I. Arriotua, T. Rojo, J. Magnetism Magnetic Mater. **164**, 251 (1996)
29. A. Yamada, H. Koizumi, N. Sonoyama, R. Kanno, Elec. Solid State Lett. **8**, A409 (2005)
30. G. Kobayashi, S.I. Nishimura, M.S. Park, R. Kanno, M. Yashima, T. Ida, A. Yamada, Adv. Funct. Mater. **19**, 395 (2009)
31. C. Delacourt, P. Poizot, J.M. Tarascon, C. Masquelier, Nature Mater. **4**, 254 (2005)
32. J.L. Dodd, R. Yazami, B. Fultz, Electrochem. Solid-State Lett. **9**, A151 (2006)
33. C. Delacourt, J. Rodriguez-Carvajal, B. Schmitt, J.M. Tarascon, C. Masquelier, Solid State Sci. **7**, 1506 (2005)
34. A. Yamada, H. Koizumi, S.I. Nishimura, N. Sonoyama, R. Kanno, M. Yonemura, T. Nakamura, Y. Kobayashi, Nature Mater. **5**, 357 (2006)
35. G. Arnold, J. Garche, R. Hemmer, C. Strobele, C. Vogler, M. Wohlfahrt-Mehrens, J. Power Sources **119**, 247 (2003)
36. S. Yang, Y. Song, P.Y. Zavalij, M.S. Whittingham, Electrochem. Comm. **4**, 239 (2002)
37. C. Delacourt, P. Poizot, M. Morcrette, J.M. Tarascon, C. Masquelier, Chem. Mater. **16**, 93 (2004)
38. C. Delacourt, P. Poizot, C. Masquelier, Electrochem. Solid-State Lett. **9**, A352 (2006)
39. C. Delacourt, C. Wurm, L. Laffont, J.B. Leriche, C. Masquelier, Solid State Ionics **177**, 333 (2006)
40. B. Ellis, W.H. Kan, W.R. Makahnouk, L.F. Nazar, J. Mater. Chem. **17**, 3248 (2007)
41. K.T. Lee, W.H. Kan, L.F. Nazar, J. Amer. Chem. Soc. **131**, 6044 (2009)
42. Z. Lu, H. Chen, R. Robert, B.Y.X. Zhu, J. Deng, L. Wu, C.Y. Chung, C.P. Grey, Chem. Mater. **23**, 2848 (2011)
43. M.-H. Lee, T.-H. Kim,Y.S. Kim, H.K. Song, J. Phys. Chem. C **115**, 12255 (2011)

44. N. Recham, L. Dupont, M. Courty, K. Djellab, D. Larcher, M. Armand, J.-M. Tarascon, Chem. Mater. **21**, 1096 (2009)
45. C. Delacourt, P. Poizot, C. Masquelier, World Patent, CNRS-UMICORE, #WO 2007/0051 (2007)
46. P. Gibot, M. Casas-Cabanas, L. Laffont, S. Levasseur, P. Carlach, S. Hamelet, J.M. Tarascon, C. Masquelier, Nature Mater. **7**, 741 (2008)
47. M. Islam, S. Driscoll, D.J. Fisher, C.A.J. Slater, P. Chem. Mater. **17**, 5085 (2005)
48. C.A.J. Fisher, M.S. Islam, J. Mater. Chem. **18**, 1209 (2008)
49. C.A.J. Fisher, V.M. Hart Prieto, M.S. Islam, Chem Mater. **20**, 5907 (2008)
50. S.Y. Chung, S.Y. Choi, T. Yamamoto, Y. Ikuhara, Phys Rev. Letters **100**, 125502 (2008)
51. S. Hamelet, P. Gibot, M. Casas Cabanas, D. Bonnin, C. Grey, J. Cabana, J.B. Leriche, J. Rodriguez Carvajal, M. Courty, S. Levasseur, P. Carlach, M. Van Thournout, J.M. Tarascon, C.J. Masquelier, Mater. Chem. **19**, 3979 (2009)
52. S. Hamelet, M. Casas-Cabanas, L. Dupont, C. Davoisne, J.M. Tarascon, C. Masquelier, Chem. Mater. **23**, 32 (2011)
53. M. Kitamura, B. Shen, S. Banno, N. Morimoto, Amer. Mineral. **69**, 154 (1984)
54. D.E. Janney, J.F. Banfield, Amer. Mineral. **83**, 799 (1998)
55. M. Armand, C. Michot, N. Ravet, M. Simoneau, P. Hovington, *European patent, EP1134 826 A1* (2001)
56. A. Abouimrane, N. Ravet, M. Armand, A. Nyten, J.O. Thomas, *Abstract #350, IMLB 12*, Nara, Japan, 27 June–2 July (2004)
57. A. Nyten, A. Abouimrane, M. Armand, T. Gustafsson, J.O. Thomas, Electrochem. Comm. **7**, 156 (2005)
58. P. Tarte, R. Cahay, C. R. Acad. Sci. **271**, 777 (1970)
59. A. Boulineau, C. Sirisopanaporn, R. Dominko, A.R. Armstrong, P. Bruce, C. Masquelier, Dalton Trans. **27**, 6310 (2010)
60. C. Sirisopanaporn, A. Boulineau, R. Dominko, D. Hanzel, A.R. Armstrong, P. Bruce, C. Masquelier, Inorg. Chem. **49**, 7446 (2010)
61. C. Sirisopanaporn, C. Masquelier, P.G. Bruce, R.A. Armstrong, R. Dominko, J. Amer. Chem. Soc. **133**, 1263 (2011)
62. S. Nishimura, S. Hayase, R. Kanno, M. Yashima, N. Nakayama, A. Yamada, J. American Chem. Soc. **130**, 13212 (2008)
63. G. Quoirin, J.M. Tarascon, C. Masquelier, C. Delacourt, P. Poizot, F. Taulelle, World Patent, WO **2008**/107571 A2
64. A.R. West, F.P. Glasser, J. Solid State Chem. **4**, 20 (1972)
65. Yamaguchi H., Akatsuka K., Acta Cryst. **B35**, 2678 (1979)
66. C. Frayret, C. Masquelier, A. Villesuzanne, M. Morcrette, J.M. Tarascon, Chem. Mater. **21**, 1861 (2009)
67. J.B. Leriche, S. Hamelet, J. Shu, M. Morcrette, C. Masquelier, G. Ouvrard, M. Zerrouki, P. Soudan, S. Belin, E. Elkaim, F. Baudelet, J. Electrochem. Soc. **157**, A606 (2010)
68. A. Senyshyna, M.J. Muhlbauera, K. Nikolowskia, T. Pirling, H. Ehrenberg, J. Power Sources **203**, 126 (2012)